STM JOURNALS

Journal of
Materials & Metallurgical Engineering

ISSN: 2231-3818 (Online)
ISSN: 2321-4236 (Print)
Volume 16, Issue 1, 2026
January–April
DOI (Journal): 10.37591/JoMME

https://journals.stmjournals.com/jomme

Research JoMME

# Mn Doping–Induced Enhancement of Ethanol Gas Sensitivity in CuO/$Cu_2O$/Cu Composites

P. Samarasekara[1,*], D.P. Gunathilake[2], D.M.S.N. Kolugala[2], P.G.D.C.K. Karunarathna[3]

***Abstract***

*A composite of CuO/Cu2O/Cu was synthesized by heating cupric acetate up to 600 °C for 2 hours in air. The properties of pure CuO films and CuO/Cu2O/Cu films were compared. Films were fabricated by the doctor blade method. Polyethylene glycol was used as a binder to prepare films. Mn was doped to composite to enhance the gas sensing properties. Compositions of Mn doped samples were confirmed using XRFS. According to XRD patterns, no peaks of Mn were actually observed in the composition, implying that Mn was successfully doped in the composite. Although there was a negligible trace amount of Cu in the composite, the ratio between amounts of CuO and Cu2O was nearly one. According to UV-Vis absorption spectra, the composite prefers to absorb lower energy photons. The gas sensitivity of the sample was measured at 400 ppm of ethanol at room temperature. The gas sensitivity of composite films at ethanol is higher than that of pure CuO. However, the variation of resistance after adsorbing ethanol behaves in opposite ways in pure CuO and composite. The gas sensitivity of the composite gradually increased from 45% to 107% with doping of Mn up to 6% of Mn. These improvements are attributed to the formation of CuO/Cu2O heterojunctions and Mn-induced defect states, which increase carrier concentration and active adsorption sites. Enhanced charge transfer and oxygen vacancy density facilitate room-temperature operation, faster response–recovery dynamics, and improved selectivity, indicating the composite's promise for low-power ethanol sensing applications with good stability and reproducibility.*

**Keywords:** CuO/$Cu_2O$/Cu composite, ethanol vapor, gas sensitivity, Mn doping, UV-Vis absorption

## INTRODUCTION

The CuO (cupric oxide) is a *p*-type semiconductor due to copper vacancies with a band gap of 1.2–1.9 eV. It finds potential applications in sensing, catalysis, energy, and electronic applications. It has a higher hole concentration compared to many other metal oxides. Among metal oxides, CuO is one of the few stable *p*-type semiconductors, which is crucial for complementary sensing and heterojunction design. Strong surface depletion/accumulation effects make conductivity highly sensitive to surface chemistry. It is highly sensitive to reducing gases such as ethanol, H2S, CO, and NH3. It possesses a low optimal operating temperature (often 150–300 °C, sometimes lower in composites). It strongly interacts with oxygen species ($O^-$, $O_2^-$) adsorbed on the surface. CuO indicates opposite sensing polarity compared to common *n*-type oxides such as ZnO or $SnO_2$.

$Cu_2O$ (cuprous oxide) is a *p*-type semiconductor due to Cu vacancies with a direct band gap of 2.0–2.2 eV. It has a higher hole mobility and longer minority carrier diffusion length. It is a prime candidate in heterostructures, optoelectronics, and gas-sensing.

***Author for Correspondence**
P. Samarasekara
E-mail: pubudus@pdn.ac.lk

[1]Senior Professor, Department of Physics, Faculty of Science, University of Peradeniya, Peradeniya, Sri Lanka
[2]Research assistant, Department of Physics, Faculty of Science, University of Peradeniya, Peradeniya, Sri Lanka
[3]Senior lecturer, Department of Nano Science Technology, Faculty of Technology, Wayamba University of Sri Lanka, Kuliyapitiya, Sri Lanka

Received Date: January 20, 2026
Accepted Date: January 28, 2026
Published Date: February 22, 2026

**Citation:** P. Samarasekara, D.P. Gunathilake, D.M.S.N. Kolugala, P.G.D.C.K. Karunarathna. Mn Doping–Induced Enhancement of Ethanol Gas Sensitivity in CuO/$Cu_2O$/Cu Composites. Journal of Materials & Metallurgical Engineering. 2026; 16(1): 52–61p.

 

Nanowires of CuO have been employed to identify ethanol vapor [1]. Core-shell nanostructures of CuO have been utilized as NO2 gas sensors [2]. Nanosheets of CuO have been applied to detect 200 ppm of ethanol, methanol, and acetone at the operating temperature 340 °C [3]. CuO films synthesized by thermal deposition method have been used to sense NO2 at the operating temperature 200 °C [4]. Films of CuO with particle size 29 nm deposited using spray pyrolysis have been employed to detect H2S at the operating temperature 250 °C [5]. Reactive dc sputtering has been utilized to grow CuO films to detect CO2 gas at the room temperature. The gas sensitivity depended on the substrate temperature and the sputtering pressure [6].

Reduced graphene oxide conjugated Cu2O nanowire mesocrystals have been employed to detect NO2 gas [7]. Cu2O/CuO microflowers have been applied to detect 5–100 ppb of NO2 at 187 °C [8]. Polyhedron hollow structured Cu2O has been utilized to sense 8.6–50 ppm ethanol at the operating temperature 210 °C [9]. Cu2O/CuO sub-microspheres were synthesized via a one step reduction approach using copper (II) acetate to detect a range of 2.1–50 ppb H2S [10]. Cu2O nanoparticles synthesized by hydrothermal reaction have been applied to detect 10 ppm of ammonia gas [11]. Cu2O/CuO nanocrystals synthesized using a hot-soap method have been employed to sense H2S [12].

In this manuscript, the gas sensitivity of Mn doped CuO/Cu2O/Cu composite in 400 ppm of ethanol vapor at room temperature is described.

## EXPERIMENTAL

Cupric acetate powder with purity 98% manufactured by Sigma Aldrich was utilized. Cupric acetate powder was heated to 600 °C for 2 hours in air to make the composite of CuO/CuO2/Cu. First 0.06 g of PEG powder was added to 8 ml of distilled water. The PEG solution was stirred 300 rpm for 15 minutes at 50 °C. Then 1.5 g of composite powder was added to 5 ml of PEG solution. Then this solution was stirred at 600 rpm for 1.5 hours at 50 °C. Then the solution was applied on glass plates to fabricate films using the doctor blade method. Films were synthesized on ITO conductive glass plates and normal nonconductive glass plates. Area of all the samples was kept at 1.5 cm × 1.7 cm. The similar procedure was followed for pure CuO powder and Mn doped composite samples. The total weight percentage of Mn was varied from 2% to 6%. Because the doping was impossible at higher Mn concentrations, the Mn concentration was increased only up to 6%.

X-Ray Diffraction (XRD) patterns of the films deposited on the nonconductive glass plates were measured using a Rigaku Ultima IV X-ray diffractometer employing Cu-Kα radiation (λ = 1.5406 Å) over a diffraction angle range of 0–50 degrees. UV-visible spectra of the films synthesized on the nonconductive glass plates were characterized by a Shimadzu 1800 UV-Vis spectrophotometer within a wavelength range of 190–1100 nm. The composition of Mn doped films was confirmed by means of a Fischeascope X ray XAN XRFS analyzer. Sheet resistances of the films grown on the nonconductive glass substrates were estimated using a Jandel RM3000+ system.

The gas sensitivity of films were prepared on the conductive side of the conductive glass plates with a central strip of conductive layer removed in order to avoid current passing through the conductive glass plate instead of the film. Two ends across the nonconductive strip were used to get the electrical contacts. Gold coated Cu wires were used as electrodes. The sample was placed in an air tight chamber. The film, a standard resistor and 5 V dc power supply are connected in series. The value of standard resistor was equal to the initial resistance of the film. A Fluke multimeter was connected parallel to the standard resistor. This voltage was measured with time after introducing the ethanol vapor to the chamber. After the complete adsorption of 570 ppm of ethanol vapor, the voltage value reached a stable value with time. Then air was passed through the chamber, and the voltage measured with time until it reached a steady value. The same procedure was followed for pure CuO, pure composites and Mn doped composite samples.

 

## RESULTS AND DISCUSSION

Figure 1 represents XRD pattern of the pure CuO film. All the peaks belong to the phase of pure CuO (JCPDS – card # 05 – 0661) with monoclinic crystal structure (tenorite phase) [13]. Figure 2 shows the XRD patterns of CuO/Cu2O/Cu composite and Mn doped composite samples. All the peaks belong to the phases of CuO, Cu2O or Cu [14, 15]. Cu2O is a material with cubic crystal structure, high crystallographic symmetry and ease of nanostructuring. Cu is a crystal with face-centered cubic structure. No extra peaks were observed in the XRD pattern after adding Mn to the composite. Addition of Mn does not alter the structure of the phase by indicating the complete doping of Mn in the lattice of the composite. Addition of 6% Mn slightly changes the intensities of some XRD peaks. The intensity of a diffracted peak fundamentally depends on the *structure factor*, which depends on the type, number, and positions of atoms in the unit cell. When a dopant is added, it changes the chemical composition and the electron density at certain crystallographic positions. Elements with more electrons scatter X-rays more efficiently than those with fewer electrons, directly affecting the peak intensities. Heating cupric acetate easily forms heterostructures with CuO, $Cu_2O$ and metallic Cu. Because only one insignificant peak of pure Cu was observed in XRD pattern, the amount of pure Cu of the film can be neglected. The ratio of CuO:Cu2O was found to be 1.055:1 using GSAS II software. The amount of CuO phase is slightly higher than that of Cu2O phase in the composite.

Crystallite size (D) and strain (ε) were estimated using the Debye-Scherrer and Williamson-Hall equations, respectively [16, 17].

$$D = \frac{0.91\lambda}{\beta co(\theta)} \quad (1)$$

$$\varepsilon = \frac{\beta cos\,(\theta)}{4} \quad (2)$$

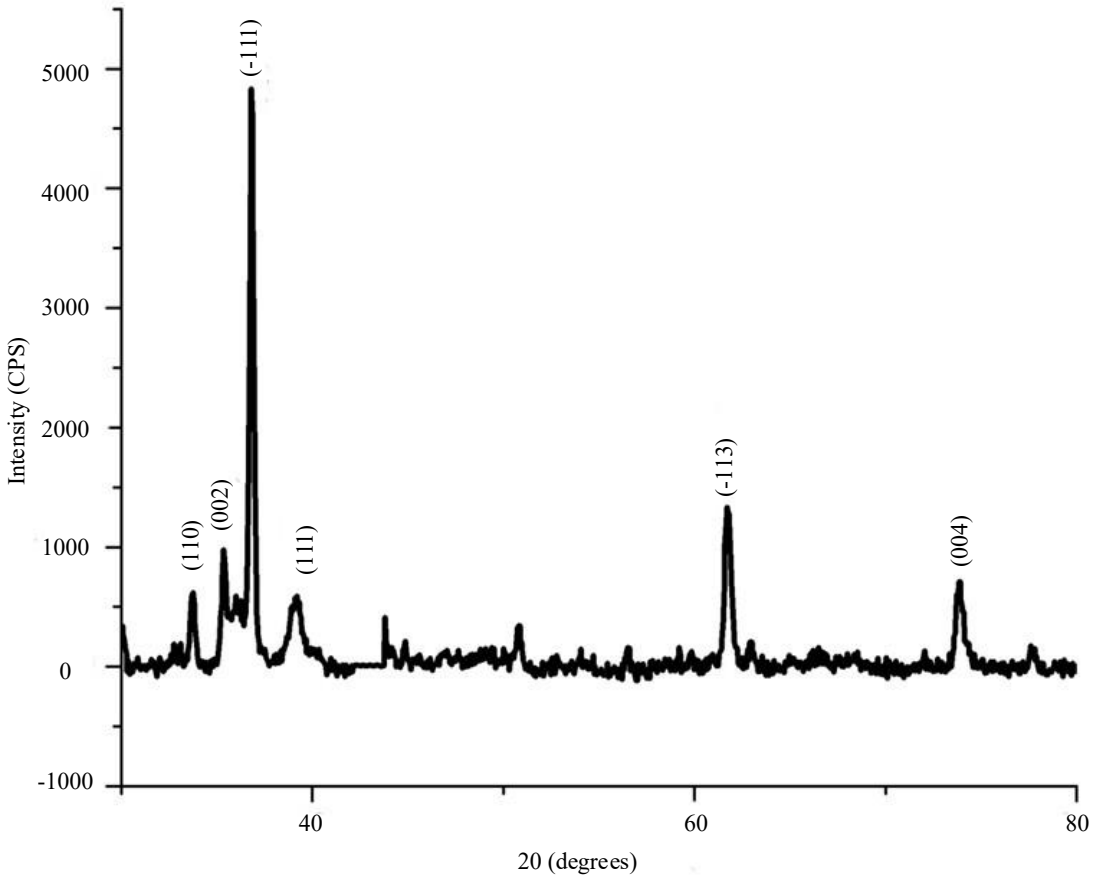


**Figure 1.** XRD pattern of pure CuO film.

 

Here, $\lambda$ represents the wavelength of Cu-Kα radiation (λ=1.5406A˚), and $\beta$ denotes the full width at half maximum (FWHM) of the XRD peak at angle $\theta$. The dislocation density ($\delta$) was determined using the relation for isotropic dislocation distributions,

$$\delta = \frac{1}{D^2} \quad (3)$$

Calculated values of crystallite size, strain, and dislocation density of pure composite, 2% Mn doped sample and 6% Mn doped sample are tabulated in table 1. These values were found for both (002) peak of CuO and (111) peak of Cu2O in each sample.

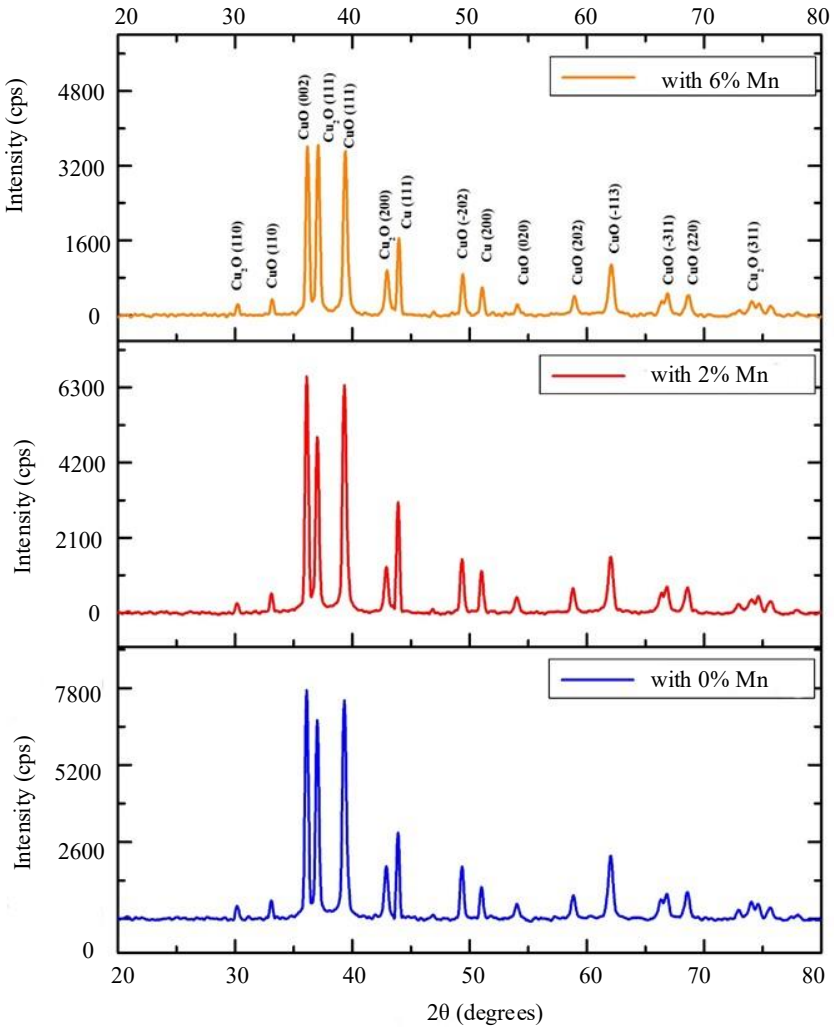


**Figure 2.** XRD patterns of CuO/Cu2O/Cu composite films with different Mn concentrations.

**Table 1.** Crystallite size, strain (□) and dislocation density (□) of CuO and Cu2O in undoped and Mn doped composites.

| | **2□□(degrees)** | **FWHM (degrees)** | **Crystallite size ($10^{-8}$ m)** | **□ ($10^{14}$ lines/m$^2$)** | **□x $10^{-3}$** |
|---|---|---|---|---|---|
| For CuO of undoped composite | 36.1 | 0.25 | 3.378 | 8.7630 | 1.0375 |
| For $Cu_2O$ of undoped composite | 37.8 | 0.25 | 3.395 | 8.6765 | 1.0324 |
| For CuO of 2% Mn doped composite | 36.1 | 0.25 | 3.378 | 8.7630 | 1.0375 |
| For $Cu_2O$ of 2% Mn doped composite | 37.6 | 0.35 | 2.423 | 17.0262 | 1.4462 |
| For CuO of 6% Mn doped composite | 36.15 | 0.25 | 3.379 | 8.7605 | 1.0374 |
| For $Cu_2O$ of 6% Mn doped composite | 37.1 | 0.25 | 3.388 | 8.7125 | 1.0345 |

 

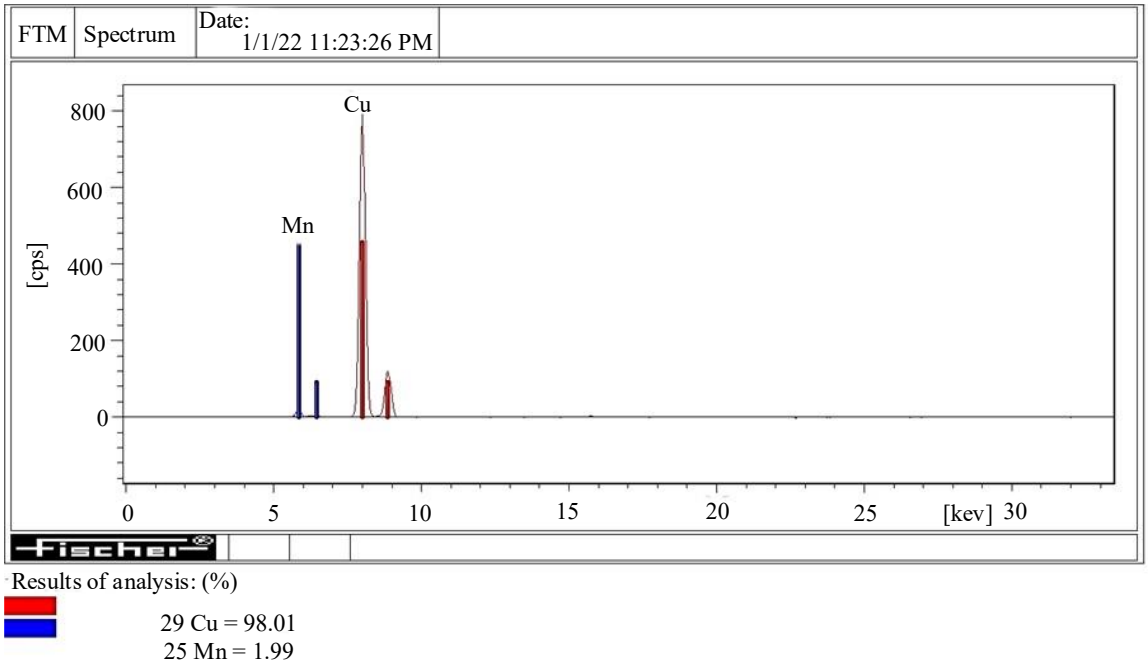


**Figure 3.** XRFS of the composite doped with 2% Mn.

Figure 3 delineates X-Ray Fluorescence Spectrum (XRFS) of the CuO/Cu2O/Cu composite doped with 2% Mn. The XRFS of other doped films also confirm the correct composition of Mn.

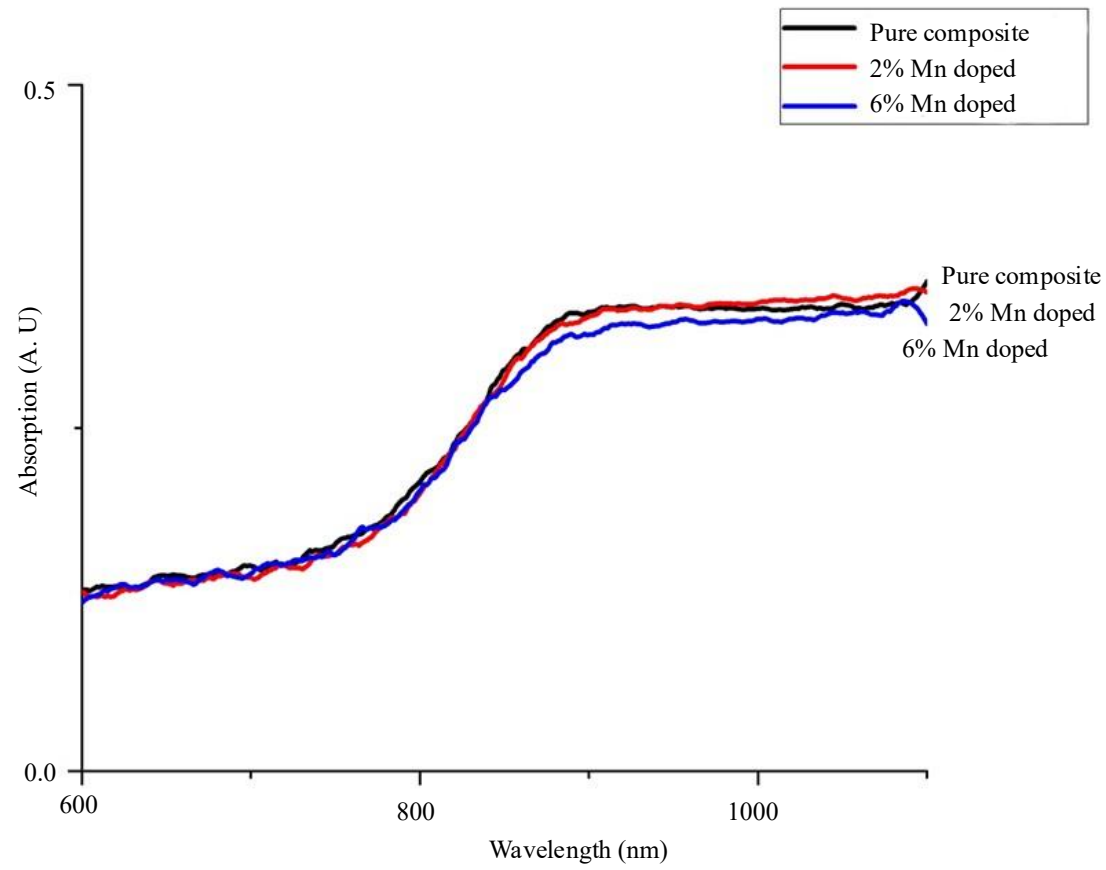


**Figure 4.** UV–Vis absorption spectra of the pure CuO/$Cu_2O$/Cu composite (black curve), 2% Mn doped composite (red curve) and 6% Mn doped composite (blue curve).

 

Figure 4 represents the UV–Vis absorption spectra of the pure CuO/$Cu_2O$/Cu composite, 2% Mn doped composite and 6% Mn doped composite. The absorption of some composites starts in the near infrared [18, 19]. The UV–Vis absorption spectra of all the films exhibit a broad absorption edge extending into the near-infrared region, indicating a reduced effective band gap compared to single-phase oxides. The gradual increase in absorbance and absence of a sharp band edge suggest the presence of interfacial defect states, band tailing, and free-carrier absorption arising from CuO/$Cu_2O$ heterojunctions and metallic Cu. These features enable enhanced low-energy photon absorption, which is beneficial for gas-sensing applications. Doping Mn does not make any significant influence on the UV- Vis absorption spectra. A slight difference between absorptions of the three spectra can be observed only at higher wavelengths.

Voltage (v) across the standard resistor (s) was measured. The current (I) through the sample and the resistance (R) of the sample are given by the following equations.

$$v = is \tag{4}$$

$$R = \left(\frac{5}{v} = 1\right) s \tag{5}$$

All the samples were measured at 400 ppm of ethanol vapor at room temperature. Figure 5 shows the graph of voltage measured across the standard resistor for pure CuO, pure CuO/$Cu_2O$/Cu composite and Mn doped composites versus time. Figure 6 represents the graph of the current through each mentioned sample versus time. Figure 7 delineates the resistance of each sample versus sample. The resistance of pure CuO sample decreases with time after adsorbing ethanol vapor, the resistance of the sample increases after removing ethanol vapor.

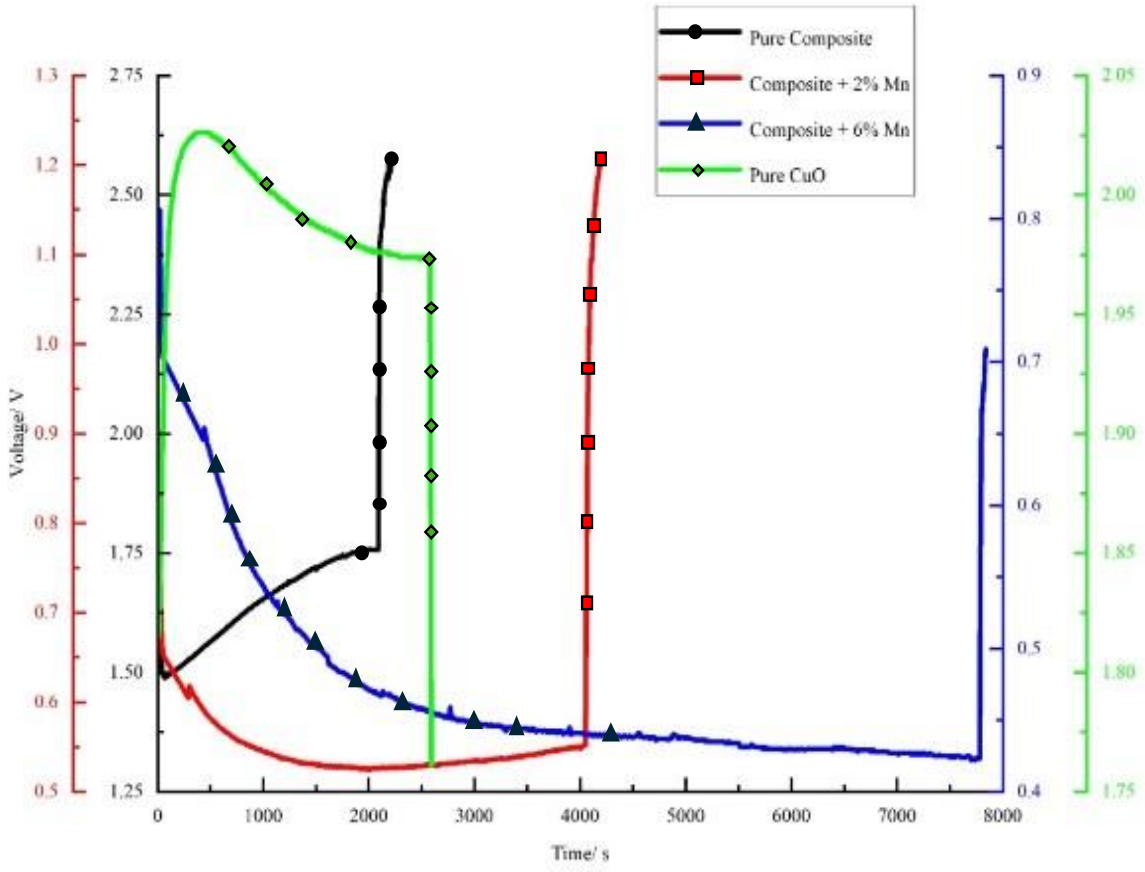


**Figure 5.** Voltage versus time of each sample measured at 400 ppm of ethanol vapor.

 

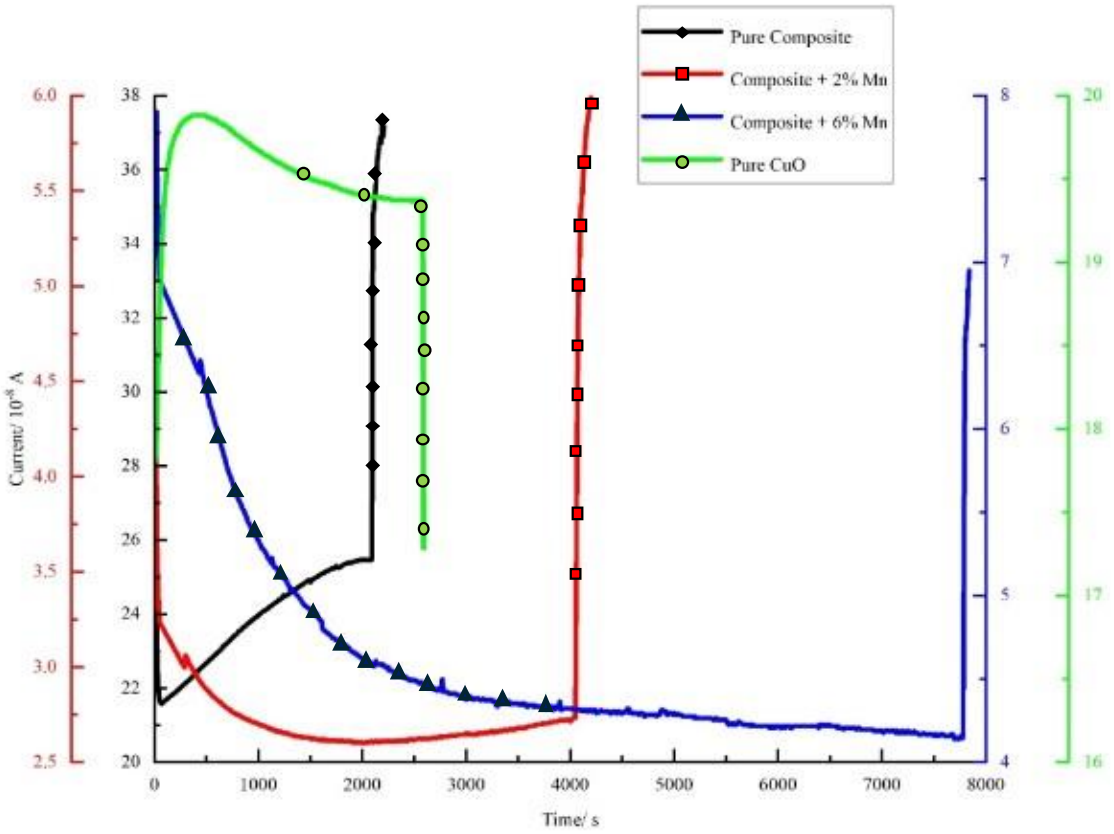


**Figure 6.** Current versus time of each sample measured at 400 ppm of ethanol vapor.

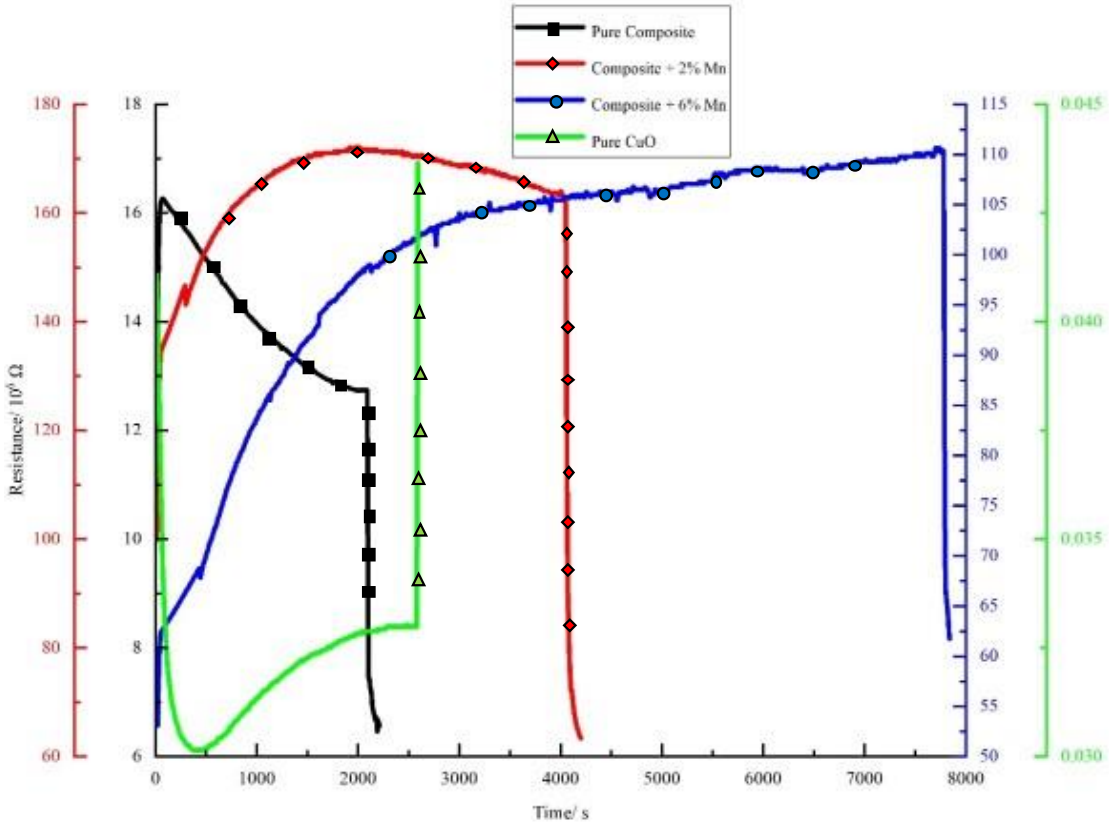


**Figure 7.** Resistance versus time of each sample measured at 400 ppm of ethanol vapor.

 

The decrease in resistance of CuO upon ethanol exposure is attributed to ethanol-induced electron donation and removal of chemisorbed oxygen, leading to surface inversion from *p*-type to *n*-type conduction and thinning of grain-boundary potential barriers, which enhances charge transport.

Ethanol removes surface oxygen species as follows.

$C2H5OH+O- \rightarrow CO2+H2O+e-$

In addition, when ethanol vapor arrives, it reacts with adsorbed oxygen as follows.

$C2H5OH+6O- \rightarrow 2CO2+3H2O+6e-$

This reaction *releases electrons back to the semiconductor.* The gas sensing properties of pure CuO measured in methanol behaved in a similar way [20].

However, the resistance of all the undoped and doped CuO/$Cu_2O$/Cu composite samples increases after adsorbing ethanol vapor. The increase in resistance upon ethanol exposure arises from electron release during ethanol–oxygen surface reactions, which compensates holes in the *p*-type CuO/$Cu_2O$ matrix and enhances interfacial barrier heights at Cu–oxide and oxide–oxide junctions.

The gas sensitivity of the samples were calculated using

$$Gas\ sensitivity = \frac{|R_f - R_i|}{R_i} x100\% \quad (6)$$

Where Ri and Rf are the initial resistance in air and the final saturated resistance after adsorbing ethanol vapor, respectively. The gas sensitivity and the response time of each sample measured at 400 ppm of ethanol vapor at room temperature are given in Table 2. The higher the gas sensitivity is the longer the response time as observed for many gas sensors.

CuO possesses high density of surface defects and oxygen vacancies. In addition CuO exhibits excellent catalytic activity for oxidation of alcohols and hydrocarbons, strong chemisorption of oxygen and organic molecules. All these properties of CuO leads to enhanced gas sensitivity, selectivity, and stability, especially for alcohol vapors like ethanol. On the other hand, Cu2O exhibits high sensitivity to reducing gases such as ethanol at lower operating temperatures than many wide band gap oxides. $Cu_2O$ often shows faster response/recovery than CuO due to lower activation energy for surface reactions. The reversible redox behavior of Cu2O enables dynamic modulation of electronic properties, which is particularly beneficial for sensing and catalysis. $Cu_2O$ acts as an intermediate energy layer, enhancing charge transport and junction modulation in composite systems. Cu2O provides enhanced charge carrier mobility, interface driven sensitivity enhancement and dynamic redox controlled conductivity. These features of Cu2O significantly improve ethanol gas-sensing sensitivity, response speed, and stability when combined with CuO and Cu [21].

The gas sensitivity of CuO/$Cu_2O$/Cu in ethanol is higher compared to that of pure CuO due to the following reasons. In the composite, *p*-*p* junctions and *p*-metal junctions can be simultaneously found. These interfaces create built in electric fields, wider depletion/accumulation regions and higher baseline resistance. When ethanol reacts at the surface, the change in barrier height and depletion width is amplified, giving a much larger resistance change than in single-phase CuO or $Cu_2O$ [22].

**Table 2.** Gas sensitivity and response time of each sample measured at 400 ppm of ethanol.

| | Gas sensitivity (%) | Response time (min) |
|---|---|---|
| Pure composite | 45 | 1 |
| 2% Mn doped composite | 73 | 30 |
| 6% Mn doped composite | 107 | 126 |
| Pure CuO | 25 | 5 |

 

When Mn is doped into $CuO/Cu_2O$, Mn exists mainly as $Mn^{2+}$ / $Mn^{3+}$. The lattice forms *oxygen vacancies to* maintain charge neutrality. These vacancies increase adsorption of oxygen ($O^-$, $O_2^-$) and provide more reactive sites for ethanol oxidation. Because ethanol is a *strong reducing gas*, more the adsorbed oxygen is the larger the resistance change. The more the released electrons is the higher the sensitivity. Mn is *catalytically active* for alcohol oxidation. Mn facilitates C–H and O–H bond breaking in ethanol, which lowers activation energy of surface reactions. Therefore, Mn provides faster reaction kinetics at lower operating temperatures. As a result, Mn-doped sensors often exhibit higher response, faster response/recovery and lower optimal sensing temperature. Ethanol has multiple reactive bonds, and it interacts strongly with metal-oxide surfaces compared to CO or NH3. $CuO/Cu_2O$ heterojunctions and CuO/Cu metal Schottky contacts can be found in $CuO/Cu_2O$/Cu composite. Mn doping alters carrier concentration (hole density), increases depletion width at interfaces, and enhances band bending. When ethanol reacts, released electrons recombine with holes, and Junction barriers collapse more dramatically. As a result, *larger resistance change can be observed in Mn doped sample* than the undoped composite [23]. Doping Mn induces higher surface roughness and more porous morphology. As a result, larger effective surface area, better gas diffusion and more grain boundaries (each acts as a sensing barrier) can be observed.

## CONCLUSION

Composite of $CuO/Cu_2O$/Cu could be successfully synthesized by heating cupric acetate. Doping of Mn did not add any extra peaks to XRD pattern of $CuO/Cu_2O$/Cu composite. According to UV-visible spectra, presence of interfacial defect states, band tailing, and free-carrier absorption arising from $CuO/Cu_2O$ heterojunctions and metallic Cu were observed. These features are favorable for gas-sensing applications. The gas sensitivity of pure composite (45%) is higher than the gas sensitivity pure CuO (25%). Enhanced charge carrier mobility, interface driven sensitivity enhancement and dynamic redox controlled conductivity of Cu2O significantly improve ethanol gas-sensing sensitivity, response speed, and stability when combined with CuO and Cu in the $CuO/Cu_2O$/Cu composite. The gas sensitivity gradually increased with doping Mn up to 8% Mn. Doping was impossible above 8% of Mn. The response time also gradually increased with Mn percentage. Mn doping enhances ethanol gas sensitivity of $CuO/Cu_2O$/Cu composites by increasing oxygen vacancy concentration, catalytic activity, and interfacial barrier modulation, leading to enhanced surface reactions and larger resistance variation upon ethanol exposure. After adsorbing ethanol vapor, the resistance of all the composite samples increases due to electrons released during ethanol–oxygen surface reactions, which compensates holes in the *p*-type $CuO/Cu_2O$ matrix and enhances interfacial barrier heights at Cu–oxide and oxide–oxide junctions.

## REFERENCES

1. Zappa D, Comini E, Sberveglieri G. Gas-sensing properties of thermally-oxidized metal oxide nanowires. *Procedia Engineering*. 2012 Jan 1;47:430–3.
2. Park S, Kim S, Sun GJ, In Lee W, Kim KK, Lee C. Fabrication and $NO_2$ gas sensing performance of $TeO_2$-core/CuO-shell heterostructure nanorod sensors. *Nanoscale Research Letters*. 2014 Nov 27;9(1):638.
3. Umar A, Alshahrani AA, Algarni H, Kumar R. CuO nanosheets as potential scaffolds for gas sensing applications. *Sensors and Actuators B: Chemical*. 2017 Oct 1;250:24–31.
4. Li Y, Liang J, Tao Z, Chen J. CuO particles and plates: synthesis and gas-sensor application. *Materials Research Bulletin*. 2008 Aug 4;43(8–9):2380–5.
5. Bari RH, Patil SB, Bari AR. Spray-pyrolized nanostructured CuO thin films for $H_2S$ gas sensor. *International Nano Letters*. 2013 Dec;3(1):12.
6. Samarasekara P, Yapa NU. Effect of sputtering conditions on the gas sensitivity of Copper Oxide thin films. *Sri Lankan Journal of Physics*. 2007 Nov 11;8(21-27)
7. Deng S, Tjoa V, Fan HM, Tan HR, Sayle DC, Olivo M, Mhaisalkar S, Wei J, Sow CH. Reduced graphene oxide conjugated $Cu_2O$ nanowire mesocrystals for high-performance $NO_2$ gas sensor. *Journal of the American Chemical Society*. 2012 Mar 14;134(10):4905–17.

 

8. Wang N, Tao W, Gong X, Zhao L, Wang T, Zhao L, Liu F, Liu X, Sun P, Lu G. Highly sensitive and selective $NO_2$ gas sensor fabricated from $Cu_2O$–CuO microflowers. *Sensors and Actuators B: Chemical*. 2022 Jul 1;362:131803.
9. Sui Y, Zeng Y, Zheng W, Liu B, Zou B, Yang H. Synthesis of polyhedron hollow structure $Cu_2O$ and their gas-sensing properties. *Sensors and Actuators B: Chemical*. 2012 Aug 1;171:135–40.
10. Meng FN, Di XP, Dong HW, Zhang Y, Zhu CL, Li C, Chen YJ. Ppb $H_2S$ gas sensing characteristics of $Cu_2O$/CuO sub-microspheres at low-temperature. *Sensors and Actuators B: Chemical*. 2013 Jun 1;182:197–204
11. Zhao K, Li X, Tang J, Yang H, Wu Q, Wang X, Guo X, Zeng D. Effect of exposed facet determined the room-temperature ammonia gas sensing of $Cu_2O$ nanoparticles. *Applied Surface Science*. 2023 Mar 15;613:156008.
12. Mikami K, Kido Y, Akaishi Y, Quitain A, Kida T. Synthesis of $Cu_2O$/CuO nanocrystals and their application to $H_2S$ sensing. *Sensors*. 2019 Jan 8;19(1):211 **[1-14]**
13. Chandrasekar M, Subash M, Logambal S, Udhayakumar G, Uthrakumar R, Inmozhi C, Al-Onazi WA, Al-Mohaimeed AM, Chen TW, Kanimozhi K. Synthesis and characterization studies of pure and Ni doped CuO nanoparticles by hydrothermal method. *Journal of King Saud University-Science*. 2022 Apr 1;34(3):101831.
14. Abd-Elkader OH, Deraz NM. Synthesis and characterization of new copper based nanocomposite. *International Journal of Electrochemical Science*. 2013 Jun 1;8(6):8614–22.
15. Wang P, Gong CH, Tang AY, Gu AT, Chen KW, Yi Y. Cu-BTC derived CuO and CuO/$Cu_2O$ composite: efficient adsorption material to iodide ions. *Materials Research Express*. 2023 Feb 20;10(2):025005.
16. Bilgin VI, Kose S, Atay FE, Akyuz I. The effect of substrate temperature on the structural and some physical properties of ultrasonically sprayed CdS films. *Materials Chemistry and Physics*. 2005 Nov 15;94(1):103–8.
17. Rathinamala I, Pandiarajan J, Jeyakumaran N, Prithivikumaran N. Synthesis and physical properties of nanocrystalline CdS thin films-influence of sol aging time & annealing temperature. *International Journal of Thin Films Science and Technology*. 2014;3(3):113–20.
18. Muheddin DQ, Aziz SB, Mohammed PA. Variation in the optical properties of PEO-based composites via a green metal complex: macroscopic measurements to explain microscopic quantum transport from the valence band to the conduction band. *Polymers*. 2023 Feb 2;15(3):771
19. Ahmed MA, Mahmoud SA, Mohamed AA. Interfacially engineered metal oxide nanocomposites for enhanced photocatalytic degradation of pollutants and energy applications. *RSC Advances*. 2025;15(20):15561–603.
20. Cretu V, Postica V, Ababii N, Magariu N, Sontea V, Schütt F, Adelung R, Lupan O. Effect of dopant on selectivity of CuO nanostructured films–Based sensors. In3rd International Conference on Nanotechnologies and Biomedical Engineering: ICNBME-2015, September 23-26, 2015, Chisinau, Republic of Moldova 2016 Jan 8 (pp. 349-352). Singapore: Springer Singapore.
21. Hsu CL, Tsai JY, Hsueh TJ. Ethanol gas and humidity sensors of CuO/$Cu_2O$ composite nanowires based on a Cu through-silicon via approach. *Sensors and Actuators B: Chemical*. 2016 Mar 1;224:95–102.
22. Maier C, Egger L, Köck A, Becker S, Niehaus JS, Reichmann K. Investigation of Gas Sensing Performance of CuO/$Cu_2O$ Thin Films as a Function of Au-NP Size for CO, $CO_2$, and Hydrocarbons Mixtures. *Nanomaterials*. 2025 May 8;15(10):705.
23. Rajapaksha RM, Samarasekara P, Karunarathna PG, Fernando CA. Improvement of gas sensitivity of ferric oxide thin films by adding Mn nanoparticles. *Bulletin of Materials Science*. 2021 Sep;44(3):182.

 